Impact of dispersive and saturable gain/loss on bistability of nonlinear parity–time Bragg gratings

Sendy Phang,[1,*] Ana Vukovic,[1] Hadi Susanto,[2] Trevor M. Benson,[1] and Phillip Sewell[1]

[1]*The George Green Institute for Electromagnetics Research, Faculty of Engineering, University of Nottingham, Nottingham NG7 2RD, UK*

[2]*Department of Mathematical Sciences, University of Essex, Colchester CO4 3SQ, UK*

**Corresponding author: sendy.phang@nottingham.ac.uk*

Received March 17, 2014; revised March 25, 2014; accepted March 25, 2014; posted March 25, 2014 (Doc. ID 208442); published April 21, 2014

We report on the impact of realistic gain and loss models on the bistable operation of nonlinear parity–time (PT) Bragg gratings. In our model we include both dispersive and saturable gain and show that levels of gain/loss saturation can have a significant impact on the bistable operation of a nonlinear PT Bragg grating based on GaAs material. The hysteresis of the nonlinear PT Bragg grating is analyzed for different levels of gain and loss and different saturation levels. We show that high saturation levels can improve the nonlinear operation by reducing the intensity at which the bistability occurs. However, when the saturation intensity is low, saturation inhibits the PT characteristics of the grating.

OCIS codes: (250.4480) Optical amplifiers; (190.0190) Nonlinear optics; (190.1450) Bistability.
http://dx.doi.org/10.1364/OL.39.002603

Optical structures with balanced gain and loss, mimicking parity and time (PT) symmetry in quantum field theory [1], have been the subject of intense investigation in the last few years. PT symmetric structures based on Bragg gratings [2–4], couplers [5,6], and lattices [7,8] have been reported and demonstrated functionalities including optical switching [4,9–11], unidirectional invisibility [2,7,12], and memory [13]. Unidirectional invisibility [7,12] and power oscillation [14] have also been experimentally demonstrated. A linear PT-symmetric Bragg grating (PTBG) has a different response for a signal incident from the left and right sides of the grating whereby the transmittances are the same, $T_L = T_R$, and the reflectances are different, $\Gamma_L \neq \Gamma_R$. It is important to note that although this is commonly referred to as a nonreciprocal behavior, in a strict sense a linear PT structure does satisfy the Lorentz reciprocity condition [15,16]. This is because the scattering matrix of the structure is complex–symmetric, $\bar{\bar{S}} = (\bar{\bar{S}})^t$, although it is no longer unitary or orthogonal, $\bar{\bar{S}} = (\bar{\bar{S}})^\dagger$, where t and $\dagger$ represent the transpose and transpose-conjugate operators, respectively. Of particular interest is the unidirectional invisibility phenomenon, which occurs when the modulation of the real and imaginary parts of the refractive index of the structure are equal, at which no reflection is observed from one side of the grating. In the case of linear and frequency-independent materials, unidirectional invisibility is present at all frequencies [2–4]. It has been suggested that the inclusion of Kerr-type nonlinearity into the PT gratings promises to open a range of new applications, or to improve the existing ones [2,9,13]. It is important to note that a few papers that considered nonlinear PT structures [2,9,17] have done so under the assumptions that the gain and loss are nonsaturable and nondispersive.

In this Letter, we extend the analysis by considering a nonlinear PTBG that has both dispersive and saturable gain and loss with the real and imaginary parts of the refractive index satisfying the Kramers–Kronigs relationship. In particular, we analyze the unidirectional operation of dispersive Bragg gratings and then extend the analysis to nonlinear PTBGs and report on how different levels of gain and loss saturation can have a crucial role in enabling or inhibiting the interplay between the PT and nonlinear behavior. For this we consider a scenario of a GaAs Bragg grating with realistic parameters of material dispersion, nonlinearity, and gain/loss saturation. For this purpose a time-stepping numerical technique based on the transmission line modeling (TLM) method [18] is used. The TLM method is a flexible time-stepping numerical technique that has been extensively characterized and used over many years [19]. However, any time-domain method, including the finite-difference time-domain (FDTD) method, could be employed for this purpose. It is appropriate to comment that the TLM method has comparable performance to the FDTD method but offers certain advantages for particular applications [19]. In our earlier work we validated the TLM method for modeling PTBGs and used it to demonstrate real-time optical switching, assuming a simple case where material and gain/loss models are frequency and intensity independent [4].

A nonlinear PTBG (NPTBG) is illustrated in Fig. 1(a). The structure is embedded in a background material with

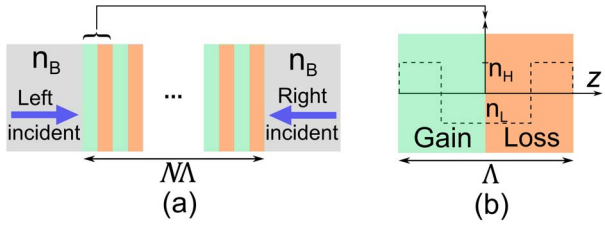

Fig. 1. (a) Schematic of an N-period PTBG in a background material n_B, (b) single period of a grating with n_H and n_L as the high and low real refractive indices at f_B in even symmetry and gain (green) and loss (orange) in odd symmetry.

a refractive index n_B and has a length of $N\Lambda$, where Λ denotes the length of a single period and N is the total number of periods. The refractive index distribution in a single period, $\hat{n}_G$, along the propagation direction z, shown in Fig. 1(b), can be expressed as

$$\hat{n}_G(z,\omega,I,t)=\begin{cases}\hat{n}_H(\omega)+n_2I(z,t)+j\frac{c}{\omega}\alpha(\omega,I), & z<\frac{\Lambda}{4}\\ \hat{n}_L(\omega)+n_2I(z,t)+j\frac{c}{\omega}\alpha(\omega,I), & \frac{\Lambda}{4}<z<\frac{\Lambda}{2}\\ \hat{n}_L(\omega)+n_2I(z,t)-j\frac{c}{\omega}\alpha(\omega,I), & \frac{\Lambda}{2}<z<\frac{3\Lambda}{4}\\ \hat{n}_H(\omega)+n_2I(z,t)-j\frac{c}{\omega}\alpha(\omega,I), & \frac{3\Lambda}{4}<z<\Lambda\end{cases}, \tag{1}$$

where $\hat{n}_H$ and $\hat{n}_L$ are the complex high and low refractive indices, which are frequency dependent, n_2 is the Kerr nonlinearity constant, I is the input signal intensity, and $\pm\alpha(\omega,I)$ denotes the gain (+) or loss (−) in the grating that is both dispersive and saturable. The complex dispersive dielectric material based on a simple harmonic oscillator model with a Lorentzian profile is implemented in the TLM method, in which the refractive index $\hat{n}$ at any frequency ω can be calculated as

$$\hat{n}^2=(1+\chi_{e\infty})+\frac{\chi_{e0}\omega_{0D}^2}{2j\omega\delta+(\omega_{0D}^2-\omega^2)}. \tag{2}$$

Here, δ and ω_{0D} denote the damping and the resonant frequency of the medium, $\chi_{e\infty}$ denotes the dielectric susceptibility at infinite frequency, and χ_{e0} is the dispersive dielectric susceptibility contribution to the overall material refractive index. Details of the implementation and validation of the material dispersion and nonlinearity in the TLM method have been reported in [20]. The Bragg frequency f_B of the grating is related to the real part of average refractive index $\bar{n}=(1/2)\mathrm{Re}(\hat{n}_H+\hat{n}_L)$ of the structure by $f_B=c/2\bar{n}\Lambda$, where c is the phase velocity of light in free space.

A saturable and dispersive gain/loss model exhibiting homogenous broadening with a Lorentzian profile is implemented in the TLM method as [21]

$$|\alpha|(\omega,I)=\mathbb{S}(I)\left(\frac{|\alpha_0|}{1+j(\omega-\omega_{0\sigma})_\tau}+\frac{|\alpha_0|}{1+j(\omega+\omega_{0\sigma})_\tau}\right). \tag{3}$$

Here, the gain/loss per unit length $|\alpha|$ is related to the imaginary part of the refractive index as $|\alpha|=(\omega/c)|n_I|$, $\omega_{0\sigma}$ denotes the atomic transitional angular frequency, τ is the dipole relaxation time parameter, and α_0 denotes the peak value of gain or loss per unit length at $\omega_{0\sigma}$. The intensity dependent function $\mathbb{S}(I)$ describes the saturation factor of the gain or loss as

$$\mathbb{S}(I)=\frac{1}{1+I/I_s}, \tag{4}$$

where I and I_S denote the input signal and saturation intensity, respectively. The saturation factor $\mathbb{S}$ varies as $0<\mathbb{S}<1$, with $\mathbb{S}=0$ denoting a high saturation level ($(I/I_s)\to\infty$), whilst $\mathbb{S}=1$ denotes the unsaturated state ($(I/I_s)\to 0$). It is important to note that the model [Eqs. (2) and (3)] satisfies the Kramers–Kronigs relationship between the real and imaginary parts of refractive index of material.

Throughout this Letter, 200 periods of a PTBG based on GaAs material are considered with the following material parameters: $\chi_{e0}=7.5$, $\omega_{0D}=4614.4$ rad/ps, and $\delta=0.0923$ rad/ps [22], with the high and low refractive indices, i.e., n_H and n_L, obtained at the Bragg frequency from the high and low dielectric susceptibilities, $\chi_{e\infty}=2.8$ and 2.5, respectively, which form the grating. It is here noted that a small change in the refractive index can be achieved by replacing a small amount of Ga by Al as [23]. For modeling purposes this small change in refractive index is represented by a different $\chi_{e\infty}$. The Kerr nonlinear constant is $n_2=2\times10^{-17}$ m^2 W^{-1} [24] throughout the structure. The gain and loss parameters are $\tau=0.1$ ps and $\omega_{0\sigma}=2116.5$ rad/ps [21], while α_0 depends on the gain and loss given. The background material refractive index of GaAs at $\omega_{0\sigma}$ is $n_B=3.626$. The periodicity of the NPTBG is designed so that the bandgap of the structure is centered at the atomic transitional frequency, i.e., $f_B=(\omega_{0\sigma}/2\pi)$, and hence $\Lambda=122.7$ nm. The unidirectional (U) operation of the PTBG happens when the gain/loss parameter $|\alpha_0|=(1/2)(\omega/c)(n_H-n_L)$ [4]. For the chosen material parameters, we obtain unidirectional operation at f_B when the gain and loss coefficient $|\alpha_0|=1460.24$ cm^{-1}. All simulations were done using the TLM method and, for good accuracy, a spatial discretization of $\Delta z=c/(96f_B)$, as reported in [4]. The frequency domain response is obtained by Fourier transformation of the time-domain signal. The TLM simulation was run for $NT=524288$ time steps, which ensured that the entire signal passed through the structure and provided a sufficient frequency-domain resolution.

Figure 2 analyzes the impact of material dispersion on the frequency domain response of a linear PTBG ($n_2=0$) at the U condition ($|\alpha_0|=1460.24$ cm^{-1}) with no gain/loss saturation ($\mathbb{S}=1$). The results of the transfer matrix (T-matrix) method with and without the dispersive material model are compared with those calculated by the TLM method. The methodology of the T-matrix method is not described in this Letter, and the reader

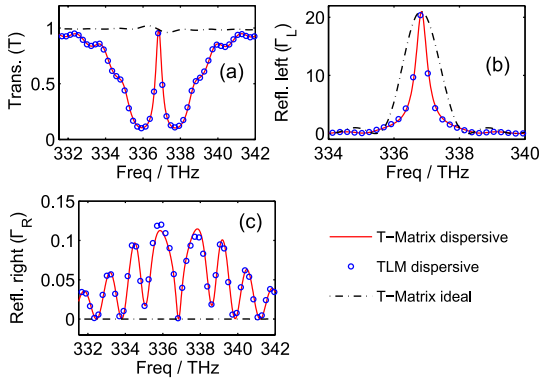

Fig. 2. (a) Transmittance and (b) reflectance for left and (c) right incidence of PTBG as a function of frequency considering a linear medium ($n_2=0$) at U condition ($|\alpha_0|=1460.24$ cm^{-1}) with no gain/loss saturation ($\mathbb{S}=1$). The results obtained using the T-matrix method for the idealized gain/loss model are included for reference.

is referred to [25]. Figure 2 shows that the results calculated by the TLM method agree well with those calculated by the T-matrix method. As expected, transmittance is the same for the left and right incidence, while the reflectances differ. More importantly, the results obtained with the dispersive material model differ significantly from those with nondispersive material parameters in that unidirectional invisibility ($T \to 1$, $\Gamma_R \to 0$) is not observed at all frequencies but is confined to a narrowband region centered at the Bragg frequency. We believe that this is an important result that limits the PT structures in real cloaking applications.

We now consider the case of an NPTBG and analyze how different levels of gain/loss saturation affect the performance of the grating. Figure 3 shows the response of the NPTBG with a high gain/loss saturation intensity of $I_S = 5 \times 10^{13}$ Wm^{-2}. Figure 3 shows transmittance T_L (a) and reflectance Γ_L (c) for the left incident and transmittance T_R (b) and reflectance Γ_R (d) for the right incident signal as a function of input signal intensity and for different gain and loss parameters $|\alpha_0|$. It is noted that for the given variation of input signal intensity, the saturation factor $\mathbb{S}$ varies as $0.3 < \mathbb{S} < 0.6$, although it is emphasized that the saturation factor throughout the structure varies due to diffraction and the presence of gain and loss. For comparison, the response of a nonlinear Bragg grating (NBG) (i.e., one without gain and loss, ($|\alpha_0| = 0$) is depicted by dashed lines. In order to obtain bistable operation, the input signal frequency is set to be at the bandgap edge [26], at which we pick a continuous wave (CW) operating at $f = 337.7$ THz. The hysteresis is obtained by gradually increasing and decreasing the input signal intensity in a single computation. This is repeated for different gain/loss parameters, that is, $|\alpha_0| =$ 800 cm^{-1} and 1460.24 cm^{-1} (U operation). It is here emphasized that U operation denotes the grating parameters and not the resulting grating response.

Figures 3(a)–3(d) show that the NPTBG is bistable for both transmittance and reflectance regardless of the side of incidence (left or right). Figures 3(a) and 3(c) show that compared to an NBG, the bistability occurs at lower input intensities for the signals incident from the left of the grating and at higher intensities for signals incident from the right side of the grating. It is noted that the transmittances for the left and right incidence are different, $T_L \neq T_R$, as shown in Figs. 3(a) and 3(b), showing that the NPTBG does not satisfy Lorentzian reciprocity. This is due to the fact that the scattering matrix is no longer a complex symmetrical matrix $\bar{\bar{S}} \neq (\bar{\bar{S}})^t$. Furthermore, it is observed that at high intensities, both Γ_L and Γ_R are very low, while transmittances are almost unity, implying bidirectional transparency [Figs. 4(c) and 4(d)].

When the NPTBG is operated with very low saturation intensity, e.g., $I_S = 65.2 \times 10^7$ Wm^{-2}, as taken from [21], and for the same input field intensity range the saturation factor varies in the range of $1.5 \times 10^{-6} < \mathbb{S} < 20 \times 10^{-6}$, it is observed that regardless of the amount of gain and loss in the system, all results overlap with that of the NBG (dashed line in Fig. 3), i.e., $T_L = T_R$ and $\Gamma_L = \Gamma_R$. This result, which is not shown separately in this Letter, confirms that when gain and loss saturation intensity are very low, PT behavior is inhibited due to the negligible effective gain and loss.

We turn our attention now to the case of no gain/loss saturation, i.e., $\mathbb{S} = 1$. Figures 4(a)–4(d) show that the NPTBG is bistable for both transmittance and reflectance regardless of the input signal incidence (from left or right side). It is noted that in the absence of gain/loss saturation, $\mathbb{S} = 1$, both the width and on/off ratio of hysteresis reduce as the gain/loss in the grating is increased. Similarly to Figs. 4(a) and 4(c), the bistability occurs at lower input intensities for the signals incident from the left of the grating compared to signals incident from the right. Of special interest is the U operation ($|\alpha_0| =$ 1460.24 cm^{-1}), at which the structure loses the hysteresis properties. Figures 4(a) and 4(b) also show that the transmittances for the left and right incidence are different, $T_L \neq T_R$, again showing that the NPTBG does not satisfy Lorentzian reciprocity. Figure 5 shows the temporal response and frequency content of the transmitted signal for the left incidence for input intensity $I = 2.6 \times 10^{14}$ Wm^{-2}, and shows the presence of longitudinal modes that fall within the gain/loss profile of the grating

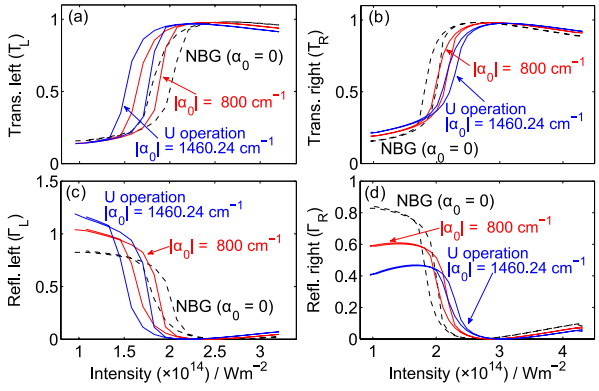

Fig. 3. Hysteresis of an NPTBG with high saturation intensity and for different gain/loss parameters $|\alpha_0| = 800$ cm^{-1} and 1460.24 cm^{-1} (U operation): (a) transmittance T_L, (c) reflectance Γ_L for the signal incident from the left; (b) transmittance T_R, (d) reflectance Γ_R or the signal incident from the right of the grating. Saturation intensity is $I_S = 5 \times 10^{13}$ Wm^{-2}. The dashed line represents the response of the NBG for reference.

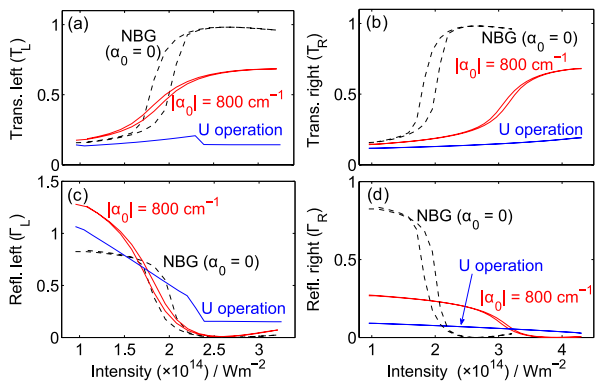

Fig. 4. Hysteresis of NPTBG operating at $f = 337.7$ THz as a function of input signal intensity for two different values of gain/loss parameters, $|\alpha_0| = 800$ cm^{-1} and 1460.24 cm^{-1} (U operation). Gain and loss saturation is turned off ($\mathbb{S} = 1$). (a) The transmittance T_L and (c) reflectance Γ_L for left incidence; (b) the transmittance T_R and (d) reflectance Γ_R for the right incidence. Hysteresis of the NBG is included for reference.

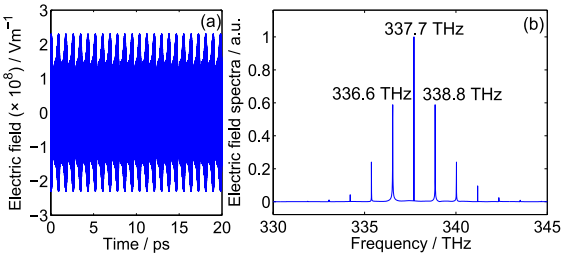

Fig. 5. (a) Time and (b) frequency response of the transmitted electric field of the NPTBG at U operation ($|\alpha_0| = 1460.24\ \mathrm{cm}^{-1}$) with input intensity $I = 2.6 \times 10^{14}\ \mathrm{Wm}^{-2}$ and the incidence from the left side of the grating.

and are spaced at multiples of ∼1.1 THz around the input signal frequency $f = 337.7$ THz. The rapid drop of T_L in Fig. 4(a) can thus be explained as a result of the transfer of energy to other frequencies.

In conclusion, we have analyzed a nonlinear GaAs-based PTBG with a full dispersive and saturable gain and loss model and have demonstrated that levels of gain/loss saturation can have a significant impact on PT behavior and should not be ignored. Low saturation intensity inhibits PT behavior and reduces the grating to a purely nonlinear grating, as we found to be the case with the gain/loss saturation intensity reported in [21]. High saturation intensity enables an interplay of nonlinear and PT phenomena, resulting in a reduction of the intensity levels at which bistability occurs. Finally, the presence of material dispersion limits the unidirectional invisibility to a narrow frequency range around the Bragg frequency and thus puts practical limits on cloaking applications.

References

1. C. M. Bender, S. Boettcher, and P. N. Meisinger, J. Math. Phys. **40**, 2201 (1999).
2. Z. Lin, H. Ramezani, T. Eichelkraut, T. Kottos, H. Cao, and D. N. Christodoulides, Phys. Rev. Lett. **106**, 213901 (2011).
3. M. Kulishov, J. M. Laniel, N. Bélanger, J. Azaña, and D. V. Plant, Opt. Express **13**, 3068 (2005).
4. S. Phang, A. Vukovic, H. Susanto, T. M. Benson, and P. Sewell, J. Opt. Soc. Am. B **30**, 2984 (2013).
5. M. Greenberg and M. Orenstein, Opt. Express **12**, 4013 (2004).
6. R. El-Ganainy, K. G. Makris, D. N. Christodoulides, and Z. H. Musslimani, Opt. Lett. **32**, 2632 (2007).
7. A. Regensburger, C. Bersch, M.-A. Miri, G. Onishchukov, D. N. Christodoulides, and U. Peschel, Nature **488**, 167 (2012).
8. K. G. Makris, R. El-Ganainy, and D. N. Christodoulides, Phys. Rev. Lett. **100**, 103904 (2008).
9. H. Ramezani, T. Kottos, R. El-Ganainy, and D. N. Christodoulides, Phys. Rev. A **82**, 043803 (2010).
10. A. A. Sukhorukov, Z. Xu, and Y. S. Kivshar, Phys. Rev. A **82**, 043818 (2010).
11. F. Nazari, M. Nazari, and M. K. Moravvej-Farshi, Opt. Lett. **36**, 4368 (2011).
12. L. Feng, Y.-L. Xu, W. S. Fegadolli, M.-H. Lu, J. E. B. Oliveira, V. R. Almeida, Y.-F. Chen, and A. Scherer, Nat. Mater. **12**, 108 (2013).
13. M. Kulishov, B. Kress, and R. Slavík, Opt. Express **21**, 9473 (2013).
14. C. E. Rüter, K. G. Makris, R. El-Ganainy, D. N. Christodoulides, M. Segev, and D. Kip, Nat. Phys. **6**, 192 (2010).
15. J. Čtyroký, V. Kuzmiak, and S. Eyderman, Opt. Express **18**, 21585 (2010).
16. D. Jalas, A. Petrov, M. Eich, W. Freude, S. Fan, Z. Yu, R. Baets, M. Popović, A. Melloni, J. D. Joannopoulos, M. Vanwolleghem, C. R. Doerr, and H. Renner, Nat. Photonics **7**, 579 (2013).
17. Z. Musslimani, K. Makris, R. El-Ganainy, and D. N. Christodoulides, Phys. Rev. Lett. **100**, 030402 (2008).
18. C. Christopoulos, *The Transmission-Line Modeling Method: TLM* (IEEE, 1995).
19. M. Krumpholz, C. Huber, and P. Russer, IEEE Trans. Microwave Theor. Tech. **43**, 1935 (1995).
20. V. Janyani, A. Vukovic, J. D. Paul, P. Sewell, and T. M. Benson, Opt. Quantum Electron. **37**, 3 (2005).
21. S. C. Hagness, R. M. Joseph, and A. Taflove, Radio Sci. **31**, 931 (1996).
22. M. Bass, G. Li, and E. van Stryland, *Handbook of Optics*, 3rd ed. (McGraw-Hill, 2010), Vol. **4**.
23. S. Adachi, J. Appl. Phys. **66**, 6030 (1989).
24. S. Lan, A. V. Gopal, K. Kanamoto, and H. Ishikawa, Appl. Phys. Lett. **84**, 5124 (2004).
25. R. E. Collin, *Field Theory of Guided Waves*, 2nd ed. (IEEE, 1991).
26. A. Suryanto, E. van Groesen, M. Hammer, and H. J. W. M. Hoekstra, Opt. Quantum Electron. **35**, 313 (2003).